



## Size-Dependent Surface Properties of Low-Reflectivity Nanoporous Alumina Thin-Film on Glass Substrate

Yi-Hao Pai,<sup>a,z</sup> Chun-Wei Tseng,<sup>a</sup> and Gong-Ru Lin<sup>b</sup>

<sup>a</sup>Department of Opto-Electronic Engineering, National Dong Hwa University, Shoufeng, Hualien, 97401, Taiwan

<sup>b</sup>Graduate Institute of Photonics and Optoelectronics, and Department of Electrical Engineering, National Taiwan University, Taipei 10617, Taiwan

The size-dependent surface properties of low-reflectivity porous alumina thin film on glass substrate produced by two-step self-organized anodization of aluminum are observed. By electro-polishing the aluminum coating, a minimum roughened surface with an  $R_{\text{rms}}$  of 3.91 nm is obtained. After adjusting the applied potential, an optimum regular structure of anodic aluminum oxide (AAO) is obtained, corresponding to the pore diameter and density of 23 nm and  $8.67 \times 10^{10} \text{ cm}^{-2}$ . In particular, nanoporous AAO with an air/solid ratio of 58% exhibits a maximum water contact angle of  $73.4^\circ$  corresponding to surface energy of  $40.1 \times 10^{-5} \text{ N cm}^{-1}$ . Furthermore, the TM-mode reflection analysis shows a diminishing Brewster angle shifted from  $60^\circ$ - $54^\circ$  with an increasing air/solid ratio from 37%-58% at 532 nm. The greatly reduced small-angle reflectance and surface energy reveals a nonlinear trend with an enlarging pore size and air/solid ratio, leading to a minimum surface reflectance and maximum water contact angle at the nanoporous AAO prepared with 60V.

© 2012 The Electrochemical Society. [DOI: 10.1149/2.009205jes] All rights reserved.

Manuscript submitted November 17, 2011; revised manuscript received January 23, 2012. Published February 14, 2012.

Nanoporous anodic aluminum oxide (AAO) membranes have a potential for technological interest in industry.<sup>1-3</sup> Notably, AAO templates with a large-range tunable inter-pore distance and pore size controlled by anodization conditions have attracted considerable attention when constructing numerous nanostructure devices, such as solar cells, batteries and sensors, due to their simple process, good thermal stability and mechanical strength.<sup>3-6</sup> Most researchers have focused almost exclusively on controlling and realizing the anodizing behavior of AAO.<sup>7-9</sup> Although it is well known that electrochemical behavior of ion migration ( $\text{Al}^{3+}$  and  $\text{O}^{2-}$ ) for porous AAO formation can conventionally be distinguished by controlling the current-time curve, the effects of geometric scale dependent reflectance on the optical properties of AAO itself have not been emphasized until recent years.<sup>2</sup> In particular, the alternative approach to simplifying anti-reflection film evaporation with lower production costs is an important key for obtaining cost-effective solar cells. More than 30% of incident light is actually reflected back from the surface of solar cells, which will decay the conversion efficiency of the solar cell.<sup>10</sup> Not long ago, Huang et al. reported an asymmetric light reflectance phenomenon for AAO films fabricated on glass substrate.<sup>11</sup> They found that the geometric asymmetry of the nanoscale aluminum networks is strongly dependent on the asymmetric light reflectance effect. Simultaneously, they indicated that such a geometric asymmetrical structure would probably induce asymmetric absorption or scattering of light from different orientations. Nevertheless, the dependence of anti-reflectance at different incident angles on the characterization of AAO has never been discussed in previous works. It is well known that self-cleaning technology is another indispensable topic that could improve water repellency as well as assist in developing multi-functional electro-optical devices, such as cover glass for solar cells or light emitting diodes. According to the literature, Tadanaga et al. show a super-water-repellent porous  $\text{Al}_2\text{O}_3$  gel coating film created by a combination of geometric and chemical approaches.<sup>12</sup> Although the porous  $\text{Al}_2\text{O}_3$  gel films provide an improved hydrophobic coating with a surface roughness different from that of the original substrate, the relationships between surface tension and porosity as well as optical properties have not yet been addressed. This study demonstrates nanoporous AAO thin films with ultra-low reflectivity and hydrophobicity on glass substrate produced by two-step anodization at room temperature. The effects of various electrochemical conditions on their geometric scale and the reflectance at different incident angles are characterized. In particular, the surface energy related hydrophobicity, as well as the

geometric scale of the electrochemical synthesized nanoporous AAO film, is investigated and elucidated.

### Experimental

The experimental parameters for fabricating nanoporous AAO film are listed below, which include glass substrate cleaning, aluminum thin-film deposition and nanoporous AAO film formation. At first, the plasma cleaning of glass substrate was performed to remove the dusty particles from the reactive-ion etcher (Trion Phantom III) at a working pressure of  $3 \times 10^{-2}$  Torr and working power of 50 watts under Ar mass flow of 40 sccm. After that, the high-purity aluminum (4N) with a film thickness of 500 nm was deposited on glass substrate by employing a thermal evaporation coat under a working pressure of  $1 \times 10^{-3}$  Torr for 15 min. Before anodization, the aluminum coated on glass substrate with working area of  $1 \text{ cm}^2$  was initially immersed in a mixed solution of phosphoric acid (85 wt%), sulfuric acid (96 wt%) and D. I. water with an electrolyte mixed volumetric ratio of 1.2:1.2:1. Simultaneously, the electro-polishing process with an operation current range from 0.1 to 0.4  $\text{mA cm}^{-2}$  was used to polish the rough surface for comparison. A minimum roughened surface of aluminum coated on glass substrate was employed in fabrication of the nanoporous AAO films. After reducing the surface irregularities of the aluminum film by fine-tuning polishing conditions, the high-purity aluminum film was treated with a two-step anodization process in a homemade anodization cell to generate ordered nanoporous AAO films. In more detail, the two-step anodization process first involved anodic oxidation and etching, and second used anodic oxidation for nanoporous AAO film formation. At the first anodic oxidation, the pretreated aluminum was immersed in 0.5 M oxalic acid solution under constant cell potential of 40 V at room temperature ( $25^\circ\text{C}$ )<sup>13</sup> to produce an early porous-alumina layer (or irregular-alumina layer). In order to improve the irregular or unusual alumina layer, the early alumina layer was etched in 0.5 M phosphoric acid at  $25^\circ\text{C}$ . The second anodic oxidation was then employed for uniform pore size generation. Note, that the second anodic oxidation process with four samples (A, B, C and D) was performed in 0.5 M oxalic acid solution under the cell potential of 30, 40, 50 and 60 V at  $25^\circ\text{C}$ , respectively.

The effect between surface roughness and applied potential of the electro-polishing process were estimated by atomic force microscopy (Gatan model 691). The surface morphologies and geometric scale of nanoporous AAO samples were characterized by field-emission scanning electron microscopy (FE-SEM, JEOL 6700F). The size and uniformity of EM images analysis are demonstrated by using related software (Digital Micrograph 3.3.1 and Origin R7.0 SRO). The

<sup>z</sup> E-mail: paiyihao@mail.ndhu.edu.tw

measurement of the water contact angle was accomplished by the sessile-drop method using a contact angle system FTA 200 (ACIL & First Ten Angstroms Inc.) and observing 15  $\mu\text{l}$  water droplets on the nanoporous AAO surface. The measurement of advancing and receding contact angles were also performed by the camera-capturing feature, simultaneously, the surface contact angle was averaged by three times and fitted with combined polynomial function. The angular dependent reflectance spectra of nanoporous AAO thin-film measured by a 532 nm laser were analyzed using a TM polarizer and a power detector. Finally, the nanoporous AAO anti-reflection coating glass for replacing traditional AR layers was fabricated upon semi-manufactured solar cells. The electric properties (short-circuit photocurrent and open-circuit voltage) of nanoporous AAO based solar cell were measured using a Keithley model 2400 source measure unit under standard conditions of AM1.5 spectra from a 500 W xenon lamp.

## Results and Discussion

To realize the effect of electro-polishing conditions as well as the smooth surface morphology, surface roughness with varying applied currents from 0.4 to 0.1  $\text{mA cm}^{-2}$  are shown in Figure 1. Obviously, the root-mean-square roughness ( $R_{\text{rms}}$ ) of polished aluminum film, with applied currents changing from 0.4–0.1  $\text{mA cm}^{-2}$ , decrease from 36.9–3.91 nm. It is speculated that with the reduction of the polishing current, the metal ions dissolve from the anode into the medium more slowly and randomly, thus, diminishing the mass transport effect to obtain a smooth aluminum. Although the removal rate of electro-polishing is greatly dependent on the electrochemical potential for the metal ions to dissolve from the anode into the medium, the surface roughness still is limited by mass transport stability,<sup>14</sup> since the degree of anisotropic etching is sensitive to metal ion migration.

Figure 2 shows the relationship between the morphological evolutions and process conditions of nanoporous AAO thin film. As the applied potential increases from 30 to 60 V, the initial current is enhanced from 0.19–0.65  $\text{mA cm}^{-2}$ , and with the reaction time increasing to 8 min, the reaction current for all samples slightly decreases with a slope varying from 0.05–0.01  $\text{mA min}^{-1}$ , corresponding to the synthesized AAO for samples D to A, respectively. According to the literature, the slope decline of current-time curves signified that in a sample there exists an oxide barrier layer between the aluminum host and the bottom of the pore, which resists chemical contact and current flow between the electrolyte and the conducting aluminum substrate, simultaneously blocking the metals in the nanopores when anodizing

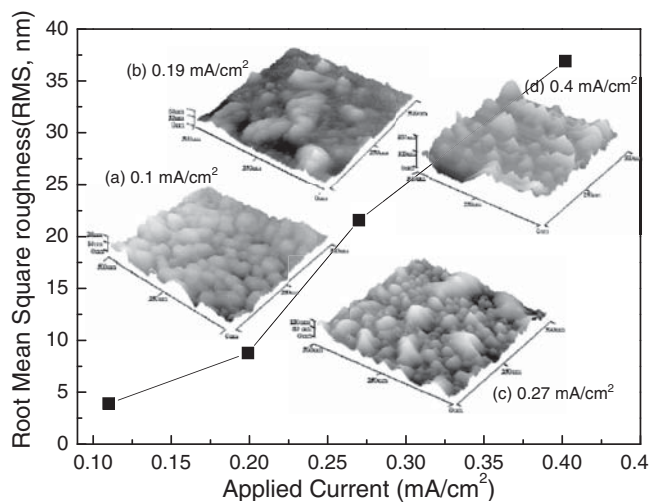


**Figure 1.** The root-mean-square roughnesses of polished aluminum film formed under anodization currents varying of (a) 0.1, (b) 0.19, (c) 0.27 and (d) 0.4  $\text{mA cm}^{-2}$ . (Inset: Topographical 3D AFM image of polished aluminum film.)

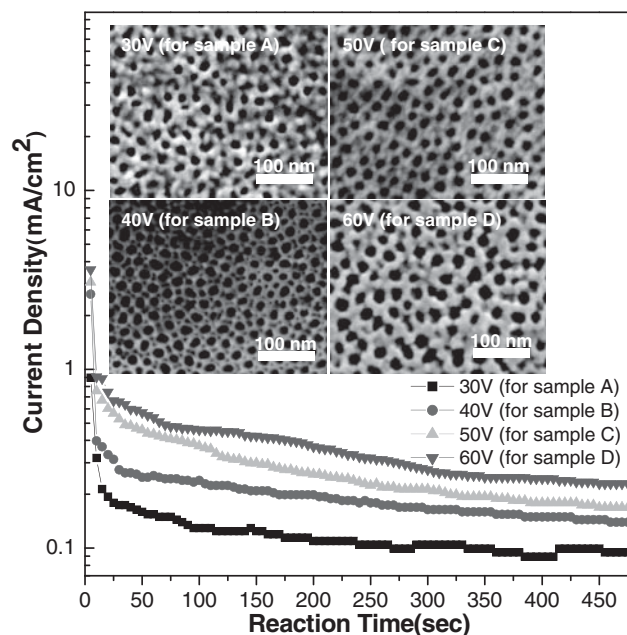


**Figure 2.** The current-time curves of nanoporous AAO thin-film formed in 0.5 M oxalic acid solution under the cell potential of 30 (for sample A), 40 (for sample B), 50 (for sample C) and 60 V (for sample D), respectively. (Inset: the SEM images of various cell potential formed AAO.)

the aluminum.<sup>15</sup> Furthermore, the various reaction potentials demonstrate the influence of the AAO structure on the surface morphology, as shown in the Figure 2 inset. In particular, nanoporous AAO using a preparation of 40 V obtains an optimal regular array as compared by using the corresponding fast Fourier Transform Analysis. The size distribution of nanoporous AAO is quantified by statistically analyzing with a previously reported method,<sup>16</sup> as shown in Figure 3. When operating at a cell potential of 30 V, the sparse AAO pore microstructure for Sample A shows an irregular pattern; the diameter and pore density are 15 nm and  $7.7 \times 10^{10} \text{ cm}^{-2}$ , respectively. As the anodization potential increases up to 40 V, the pore density reaches its maximum, corresponding to a pore diameter of 23 nm. However, the pore density decreases and diameter increases with varied cell potential from 40V to 60V, ascribing severe anodizing to the aluminum to lead to a combination of adjacent pores; this is quite similar to the phenomenon observed by Virk.<sup>17</sup> Na et al. also indicated that the cell potential was an important factor in controlling the size and the regularity of the nanoporous AAO array, which is dependent on the diffusion of both  $\text{O}^{2-}$  and  $\text{Al}^{3+}$  ions.<sup>18</sup>

To realize the relationship between the hydrophobicity and surface morphology, a water contact angle analysis was employed. Contact angle " $\theta$ " is defined geometrically as the angle formed by a liquid at the three phase boundary (a liquid, gas and solid intersect). At equilibrium, the chemical potential in the three phases should be equal. The equation can be rewritten as the Young equation:

$$\gamma_{\text{lg}} \cos \theta_{\text{c}} = \gamma_{\text{sg}} - \gamma_{\text{sl}} \quad [1]$$

where the  $\theta_{\text{c}}$  is the equilibrium contact angle,  $\gamma_{\text{sg}}$ ,  $\gamma_{\text{sl}}$  and  $\gamma_{\text{lg}}$  denote the solid–vapor, solid–liquid and liquid–vapor interfacial energy, respectively. Among them, the equilibrium  $\theta_{\text{c}}$  can be determined from advancing contact angle and receding contact angle, which can be written as:<sup>19,20</sup>

$$\cos \theta_{\text{c}} = (\gamma_{\text{A}} \cos \theta_{\text{A}} + \gamma_{\text{R}} \cos \theta_{\text{R}}) / (\gamma_{\text{A}} + \gamma_{\text{R}}) \quad [2]$$

where the  $\gamma_{\text{A}}$  is  $[\sin^3 \theta_{\text{A}} / (2 - 3 \cos \theta_{\text{A}} + \cos^3 \theta_{\text{A}})]^{1/3}$  and  $\gamma_{\text{R}}$  is  $[\sin^3 \theta_{\text{R}} / (2 - 3 \cos \theta_{\text{R}} + \cos^3 \theta_{\text{R}})]^{1/3}$ .

In Figure 4, with the preparation of nanoporous AAO at applied potentials varying from 30 to 60 V, it is observed that the water contact

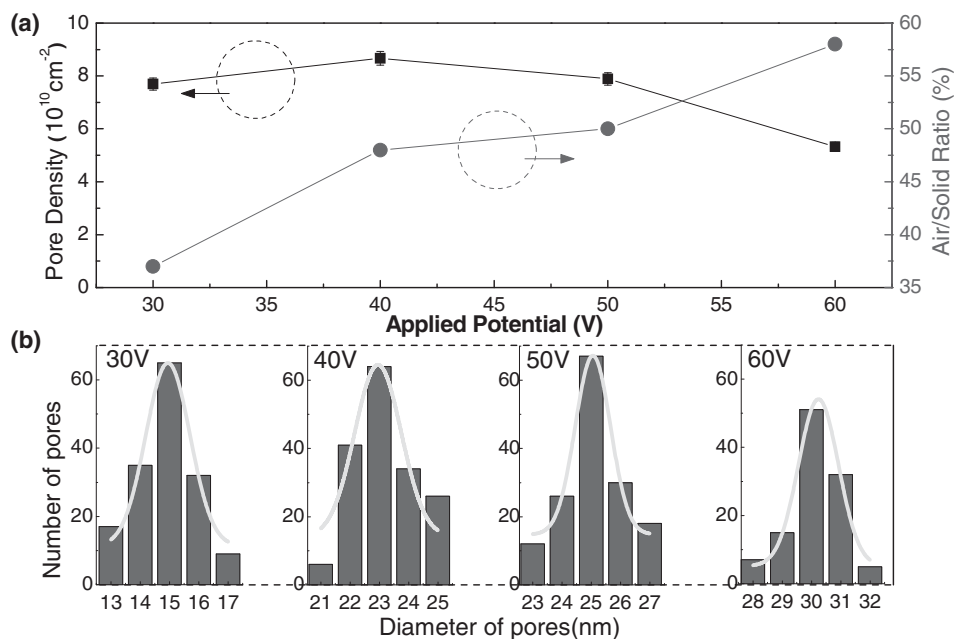


**Figure 3.** (a) Pore density and air/solid ratio as a function of the nanoporous AAO thin-film formed in 0.5 M oxalic acid solution under the cell potential of 30 (for sample A), 40 (for sample B), 50 (for sample C) and 60 V (for sample D), respectively. (b) Statistical analysis of AAO pore diameter.

angle obviously increases from  $53.13^\circ$ – $73.4^\circ$ , corresponding to the variation in the air/solid ratio from 37%–58%. Note that a water drop is easily suspended on the surface with either individual hydrophobic material coating or surface-roughening structure. Although the nanoporous AAO, prepared with 40 V, provides a maximum pore density, this result is not fully efficient and results in hydrophobic properties, whereas the water contact angle of nanoporous AAO prepared with 60 V exhibits the maximum value of  $73.4^\circ$ . Apparently, the air/solid ratio of nanoporous AAO plays a more important role in dominating the hydrophobicity than the two-dimensional density of the nanopore, since a surface with high roughness and dense structure is a relatively trivial effect to create to promote water contact. The surface energy shown in Figure 4 was calculated by using Chibowski's Formula.<sup>21</sup> The lower surface energy ( $40.1 \times 10^{-5} \text{ N cm}^{-1}$ ) with a higher contact angle ( $73.4^\circ$ ) is obtained after anodizing using 60 V; whereas the higher surface energy ( $52.7 \times 10^{-5} \text{ N cm}^{-1}$ ) leads to the lowest contact angle ( $53.1^\circ$ ) after decreasing the cell potential to 30 V. Shortening the applied potential results in a low air/solid ratio and low pore density in nanoporous AAO on a glass surface; it leads

to higher surface energy much closer to that of a plain  $\text{Al}_2\text{O}_3$  surface ( $54.2 \times 10^{-5} \text{ N cm}^{-1}$ ).

The optical transmission of nanoporous AAO with applied potentials varying from 30 to 60 V is characterized, as shown in Figure 5. The average optical transmission of all samples is over 80% in the visible range (400–700 nm). Among them, the nanoporous AAO with 40 V applied exhibits the highest optical transmission of 90% due to a relatively regular pattern. Lin et al. indicated that inhomogeneous material, with a roughened surface, enables the depolarization of the incident light at all angles of incidence, which leads to multiple scattering.<sup>22</sup> Therefore, appropriate control on structural regularity is mandatory for obtaining high optical transmission. The incident angle-dependent reflectance spectra of nanoporous AAO measured under a TM polarized incident light at 532 nm is shown in the Figure 5 inset. After sculpturing the nanoporous AAO with pore diameters enlarging from 15–30 nm, the TM mode reflectance at small incident angles is reduced from 10%–2.4%. In particular, with the formation of nanoporous AAO, the Brewster angle shifts from  $60^\circ$ – $54^\circ$  as the air/solid ratio of

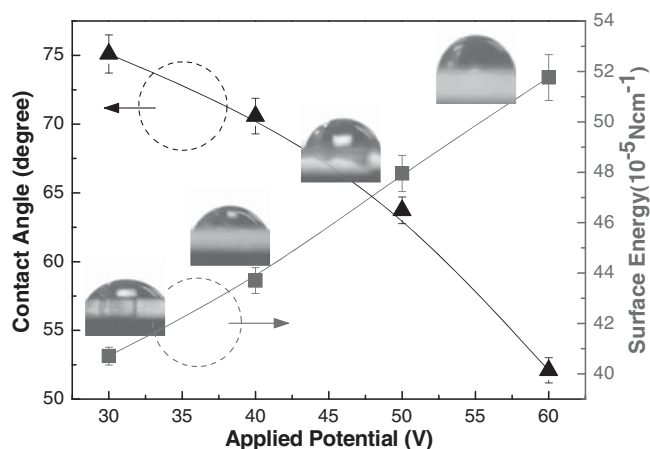


**Figure 4.** Contact angle and surface energy as a function of the nanoporous AAO thin-film formed in 0.5 M oxalic acid solution under the cell potential of 30 (for sample A), 40 (for sample B), 50 (for sample C) and 60 V (for sample D), respectively. (Inset: Photo image of the water contact angle analysis.)

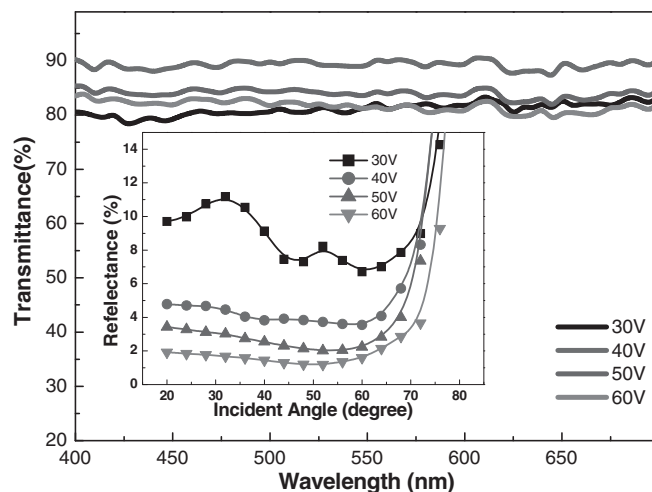


**Figure 5.** Transmission spectra of nanoporous AAO formed under the cell potential of 30 (for sample A), 40 (for sample B), 50 (for sample C) and 60 V (for sample D), respectively. (Inset: the plots of reflectance versus incident angle.)

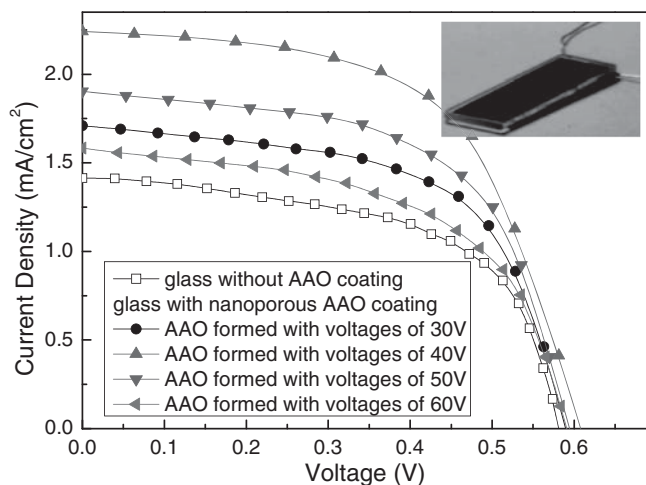


**Figure 6.** I-V curves of nanoporous AAO anti-reflection coating glass for Si based solar cells.

nanoporous AAO increases from 37%-58%, which is mainly contributed to by the combining effects of air/ $\text{Al}_2\text{O}_3$  mixed structures. The results also indicate that the air/solid ratio is an important factor for determining the minimum reflectance at arbitrary angles.

Based on above results, the wettability of a nanoporous AAO structure can be changed by adjusting of the surface energy of the solid surface. In present work, extending the applied potential results in a high air/solid ratio and low pore density in nanoporous AAO; it leads to lower surface energy since the water drop is then partially sitting on air. In addition, the irregular AAO networks also cause the asymmetric light reflectance effect, which induces asymmetric scattering or absorption of light from different orientations. This means that the air/solid ratio is great enough to give a water-repellent surface, while the nanoporous structure is too small to scatter visible light.

To investigate whether a self-organized AAO coating could improve the reflectance and the power efficiency for the solar cells, the nanoporous AAO anti-reflection coating glass were fabricated and measured upon semi-manufactured solar cells, as shown in Figure 6. From this results, the  $J_{sc}$  and  $V_{oc}$  of the nanoporous AAO anti-reflection coating glass covered semi-manufactured solar cells increase (from 1.89  $\text{mA}/\text{cm}^2$  and 0.59V to 2.26  $\text{mA}/\text{cm}^2$  and 0.617 V) with the decrease of reflectance from 10% to 5%. Furthermore, it is indicated that the  $J_{sc}$  and  $V_{oc}$  slightly drop as irregular AAO networks formation. This can be explained the asymmetric light reflectance effect, which induces asymmetric scattering or absorption of light from different orientations. The optimum  $\eta$  (1.13%) of the nanoporous AAO coating glass covered semi-manufactured solar cell is obtained by the nanoporous AAO prepared with cell potential of 40 V.

### Conclusions

The low-reflectivity porous alumina thin-film on glass substrate has demonstrated by two-step self-organized anodization of aluminum. By

controlling the applied current down to 0.1  $\text{mA}/\text{cm}^2$ , the minimum roughness of aluminum film with  $R_{rms}$  of 3.91 nm is obtained. With the preparation of nanoporous AAO at applied potentials changing from 30 to 60 V, it is found a nonlinear variation of the generated sizes with the applied potential, indicating that the size of nanoporous AAO is effectively extended between 15, 23, 25 and 30 nm, corresponding to the air/solid ratio of 37%, 48%, 50% and 58%, respectively. The water contact angle of nanoporous AAO with 60 V prepared exhibits the maximum value of 73.4° corresponding to the surface energy of  $40.1 \times 10^{-5} \text{ N}/\text{cm}^2$ . On the other hand, the nanoporous AAO with applied potential of 40V prepared exhibits highest optical transmission of 90% due to a relatively regular pattern to relax the light scattering. The TM mode reflectance of the nanoporous AAO with average pore size of 23 nm at small incident angles decrease by 80% as compared to that of the aluminum substrate, which further decay to 2.4% of its original reflectance as the porous alumina with pore size increases to 30 nm. Furthermore, an optimum power efficiency of 1.13% is obtained in the nanoporous AAO anti-reflection coating glass covered semi-manufactured solar cell.

### Acknowledgments

This work was supported in part by the National Science Council (NSC) of the Republic of China, under grants NSC 100-2218-E-259-001 and NSC 99-2218-E-259-002.

### References

- S. Lazarouk, Z. XIE, V. Chigrinov, and H. S. Kwok, *Jap. J. Appl. Phys.*, **46**(7), 4390 (2007).
- T. S. Shih, P. S. Wei, and Y. S. Huang, *Surf. Coat. Technol.*, **202**, 3298 (2008).
- B. O'Regan and M. Gratzel, *Nature (London)*, **353**, 737 (1991).
- H. Wang, C. C. Oey, A. B. Djuricic, M. H. Xie, Y. H. Leung, K. K. Y. Man, W. K. Chan, A. Pandey, J. M. Nunzi, and P. C. Chui, *Appl. Phys. Lett.*, **87**, 023507 (2005).
- J. Li, Z. Tang, and Z. Zhang, *Electrochem. Solid-State Lett.*, **8**, A316 (2005).
- O. K. Varghese, D. Gong, M. Paulose, K. G. Ong, E. C. Dickey, and C. A. Grimes, *Adv. Mater. (Weinheim, Ger.)*, **15**, 624 (2003).
- G. E. Thompson, R. C. Furneaux, G. C. Wood, J. A. Richardson, and J. S. Goode, *Nature*, **272**, 433 (1978).
- G. C. Wood, J. P. O'Sullivan, and B. Vaszko, *J. electrochem. Soc.*, **115**, 618 (1968).
- P. Skeldon, G. E. Thompson, S. J. Garcia-Vergara, L. Iglesias-Rubianes, and C. E. Blanco-Pinzon, *Electrochem. Solid State Lett.*, **9**, 47 (2006).
- W. Wang and H. Hao, *Chin. Opt. Lett.*, **8**, 35 (2010).
- K. Huang, Y. Li, Z. Wu, C. Li, H. Lai, and J. Kang, *Opt. Express* **19**(2), 1301 (2011).
- K. Tadanaga, N. Katata, and T. Minami, *J. Am. Ceram. Soc.*, **80**(4), 1040 (1997).
- M. T. Wu, I. C. Leu, and M. H. Hon, *J. Vac. Sci. Technol. B*, **20**(3), 776 (2002).
- Y. H. Pai and G. R. Lin, *J. Electrochem. Soc.*, **158**(8), E88 (2011).
- Z. F. Zhou, Y. C. Zhou, Y. Pan, and X. G. Wang, *Mater. Lett.*, **62**, 3419 (2008).
- Y. H. Pai and G.-R. Lin, *Opt. Express*, **19**(2), 896 (2011).
- R. S. Virk, "Study of Voltage, Acid Concentration, and Temperature on Nanopore Attributes of Anodized Aluminum", San Jose State Univ. San Jose (2005) pp.3-4.
- Y. Na, U. Farva, S. M. Cho, and C. Park, *Korean J. Chem. Eng.*, **26**(6), 1785 (2009).
- R. Tadmor, *Langmuir*, **20**(18), 7659 (2004).
- E. Chibowski, *J. Colloid Interf. Sci.*, **319**, 505 (2008).
- E. Chibowski, *Adv. Colloidal. Interface Sci.*, **103**, 149 (2003).
- G.-R. Lin, F. S. Meng, Y. H. Pai, Y. C. Chang, and S. H. Hsu, *Opt. Express*, **17**(23), 20824 (2009).